systems capable of introducing lymphokine genes into primary human tumor explant cultures established at the time of surgery. The development of high-efficiency retroviral vectors (*15*) makes this feasible.

REFERENCES AND NOTES

1. J. Marx, *Science* **244**, 813 (1989); G. Mathe, *Adv. Cancer Res.* **14**, 1 (1971).
2. H. B. Hewitt, E. R. Blake, E. S. Walder, *Br. J. Cancer* **33**, 241 (1976).
3. A. M. Townsend *et al.*, *Cell* **44**, 959 (1986); J. L. Maryanski, P. Pala, J. Corradin, B. B. Jordan, J. C. Cerrotini, *Nature* **324**, 578 (1986); M. M. Moore, F. R. Carbone, M. J. Bevan, *Cell* **54**, 777 (1988).
4. E. R. Fearon and B. V. Vogelstein, *Cell* **61**, 759 (1990).
5. C. Lurquin *et al.*, *ibid.* **58**, 293 (1989).
6. E. R. Fearon *et al.*, *ibid.* **60**, 397 (1990).
7. W. E. Paul and J. Ohara, *Annu. Rev. Immunol.* **5**, 429 (1987); R. Fernandez-Botran *et al.*, *Proc. Natl. Acad. Sci. U.S.A.* **83**, 9689 (1986); J. Hu-Li *et al.*, *J. Exp. Med.* **165**, 157 (1987); M. Widmer and K. Grabstein, *Nature* **326**, 795 (1987); G. Trenn, H. Takayama, J. Hu-Li, W. E. Paul, M. V. Sitkovsky, *J. Immunol.* **140**, 1101 (1988).
8. M. J. Grusby *et al.*, *Cell* **60**, 451 (1990).
9. G. P. Murphy and W. J. Hrushesky, *J. Natl. Cancer Inst.* **50**, 1013 (1973); R. R. Salup, R. B. Herberman, R. H. Wiltrout, *J. Urol.* **134**, 1236 (1985).
10. DNA was introduced into cells as a coprecipitate with calcium phosphate [F. L. Graham and A. J. van der Eb, *Virology* **52**, 456 (1973); M. Wigler *et al.*, *Proc. Natl. Acad. Sci. U.S.A.* **76**, 1373 (1979)]. The Renca–IL-4C cell line was obtained by transfection with 5 μg of the plasmid vector pBCMG-hygro–IL-4, a bovine papilloma virus expression vector containing a murine IL-4 cDNA clone under the transcriptional control of a cytomegalovirus promoter with a rabbit beta-globin intron, splice, and poly(A) addition signals; it also contains the hygromycin-resistance gene [H. Karasuyama and F. Melchers, *Eur. J. Immunol.* **18**, 97 (1988)]. The CT26–IL-4A line was derived in the same way. CT26–IL-4B was derived from CT26–IL-4A by an additional selection step in hygromycin (4 mg/ml) to generate a line that secreted similar amounts of IL-4 as Renca–IL-4C.
11. Supernatants of transfected cells (5×10^5 cells per well plated in a 24-well plate with 1.5 ml of media for 24 hours) were assayed for IL-4 by transferring dilutions of tumor cell–conditioned media to 96-well microtiter plates containing 3000 CT4S cells per well. After 48 hours, ^{3}H-thymidine was added for 12 hours after which incorporation was assessed with a PHD cell harvester. Units per milliliter of IL-4 were calculated as the reciprocal of the supernatant dilution giving half-maximal proliferation of CT4S.
12. Anti–IL-4 treatments were done with 1 mg of 11B11 MAb [J. Ohara and W. E. Paul, *Nature* **315**, 333 (1985)] injected intraperitoneally three times per week.
13. R. I. Tepper, P. K. Pattengale, P. Leder, *Cell* **57**, 503 (1989).
14. P. Golumbek and D. Pardoll, unpublished data.
15. R. Mann, R. C. Mulligan, D. Baltimore, *Cell* **33**, 153 (1983); R. C. Mulligan, in *Etiology of Human Disease at the DNA Level*, J. Lindsten and U. Petterson, Eds. (Raven, New York, 1991), p. 143.
16. T. M. Springer, G. Galfre, D. S. Secher, C. Milstein, *Eur. J. Immunol.* **9**, 301 (1979).
17. W. L. Havran *et al.*, *Nature* **330**, 170 (1987).
18. D. M. Dialynas *et al.*, *J. Immunol.* **131**, 2445 (1983).
19. M. Sarmiento, A. Glasebrook, F. Fitch, *J. Immunol.* **125**, 2665 (1980).

20. We thank G. Dranoff, R. Mulligan, W. Paul, B. Vogelstein, E. Fearon, J. Simons, and M. Howard for advice. Supported in part by the M. L. Smith Charitable Trust. D.M.P. is a recipient of the Cancer Research Institute–Benjamin Jacobson Family Investigator Award and the RJR Nabisco Research Scholars Award.

17 June 1991; accepted 9 September 1991

Functional Mapping of the Human Visual Cortex by Magnetic Resonance Imaging

J. W. BELLIVEAU,* D. N. KENNEDY, R. C. MCKINSTRY, B. R. BUCHBINDER, R. M. WEISSKOFF, M. S. COHEN, J. M. VEVEA, T. J. BRADY, B. R. ROSEN

Knowledge of regional cerebral hemodynamics has widespread application for both physiological research and clinical assessment because of the well-established interrelation between physiological function, energy metabolism, and localized blood supply. A magnetic resonance technique was developed for quantitative imaging of cerebral hemodynamics, allowing for measurement of regional cerebral blood volume during resting and activated cognitive states. This technique was used to generate the first functional magnetic resonance maps of human task activation, by using a visual stimulus paradigm. During photic stimulation, localized increases in blood volume (32 ± 10 percent, $n = 7$ subjects) were detected in the primary visual cortex. Center-of-mass coordinates and linear extents of brain activation within the plane of the calcarine fissure are reported.

PHYSIOLOGICAL, ANATOMICAL, AND cognitive psychophysical studies indicate that the brain possesses anatomically distinct processing regions (*1, 2*). During cognitive task performance, local alterations in neuronal activity induce local changes in metabolism and cerebral perfusion [blood flow and, as shown here, blood volume (*3*)]. These changes can be used to map the functional loci of component mental operations (*4*). Because the cerebral hemodynamic state in nonactivated brain areas is quite stable over time, a resting-state perfusion image can be subtracted from a stimulated-state image to create a new functional map depicting local changes caused by the activation task (*5*). To date, these functional maps have relied on radionuclide techniques [primarily positron emission tomography (PET)] that suffer from limited spatial and temporal resolution. Although accurate center-of-mass coordinates of activated regions have been obtained, the extent of cortex involved in a given task cannot be determined precisely, and distributed regions separated by less than the full width at half maximum (FWHM) resolution of the instrument cannot be resolved individually (*6*). In comparison, nuclear magnetic resonance (NMR) imaging (or MRI) is a high-resolution in vivo method for studying human cerebral anatomy (7). Recent advances in scanning speed, coupled with approval of contrast agents for human use, have yielded NMR techniques for quantitative imaging of cerebral blood volume (CBV) (*8*).

We investigated the human visual cortex using photic stimulation, a robust stimulus that produces regional changes in cerebral blood flow (CBF) of at least 30 to 50% (*5, 9*). Dynamic susceptibility–contrast NMR imaging of an intravenously administered paramagnetic contrast agent [0.5 M, gadolinium diethylenetriaminepentaacetic acid, $Gd(DTPA)^{2-}$] was used to produce regional CBV maps of the human brain during resting and activated states (*8, 10*). CBV maps were correlated directly to high-resolution (T1-weighted) three-dimensional (3-D) images of the underlying anatomy, allowing for precise determination of gray-white matter boundaries and activated-nonactivated borders. Functional CBV and anatomic data sets were translated into proportionately measured stereotactic coordinates relating to the line between the anterior and posterior commissures (AC-PC line) (*11*). This translation allows direct correlation to reported standardized PET maps of the visual cortex (*5, 9*).

Seven normal subjects underwent dynamic NMR imaging with a prototype high-speed imaging device (1.5-T GE Signa, modified by Advanced NMR Systems, Inc., Wilmington, MA) based on a variation of the echo planar imaging (EPI) technique first described by Mansfield [in (*12*)]. Light-proof, patterned-flash stimulating goggles (Model S10VS, Grass Instruments, Quincy, MA) were placed over the subject's eyes. The stimulus rate was fixed for predicted maximum CBF response (*5*) at 7.8 Hz. A snugly fitting head holder was used to minimize subject movement between scans. A surface radio frequency (r.f.) coil over the occipital pole was used to improve signal-to-noise over the posterior half of the brain.

J. W. Belliveau, R. C. McKinstry, B. R. Buchbinder, R. M. Weisskoff, M. S. Cohen, J. M. Vevea, T. J. Brady, B. R. Rosen, Massachusetts General Hospital–NMR Center, Department of Radiology, Massachusetts General Hospital and Harvard Medical School, Boston, MA 02114.

D. N. Kennedy, Massachusetts General Hospital–NMR Center, Departments of Radiology and Neurology, Massachusetts General Hospital and Harvard Medical School, Boston, MA 02114.

*To whom correspondence should be addressed, at Massachusetts General Hospital–NMR Center, 13th Street, Charlestown, MA 02129.

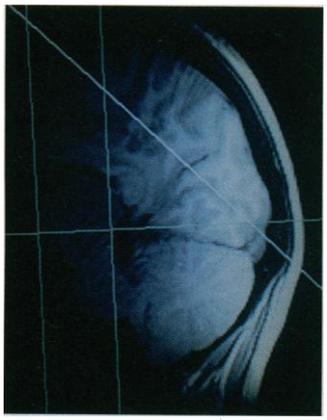

Fig. 1. Magnetic resonance surface coil image of the occipital pole. 3-D (T1-weighted) images were acquired for anatomical correlation with the functional CBV images (Fig. 3). The two vertical lines bisect the anterior and posterior commissures. A horizontal line is drawn between them (AC-PC or bicommissural line). The oblique line defines the plane of the CBV images, located along the bank of the calcarine fissure.

Sagittal slices from a 3-D (T1-weighted) data set (1 by 1 by 1.5 mm) were used to identify the plane of the calcarine fissure bilaterally (Fig. 1). We derived functional CBV maps from a series of images (60 images in 45 s) oriented in the plane of the calcarine fissures, collected at 750-ms intervals using a lipid-suppressed, spin echo EPI pulse sequence (echo time, TE = 100 ms; repetition time, TR = 750 ms; 64-ms image acquisition window) before, during, and after contrast agent injection. A slice thickness of either 8 or 10 mm was used (FWHM, sinc-shaped r.f. slice excitation for square slice profile), with an in-plane voxel size of either 1.5 by 1.5 mm or 3 by 3 mm defined by the gradient waveforms used for encoding. Using a power injector (Medrad, Pittsburgh, PA), we administered two doses of 0.1 mmol/kg $Gd(DTPA)^{2-}$, with and without 7.8-Hz photic stimulation, as a 4-s bolus into the antecubital vein.

Figure 2 displays the measured NMR signal changes in a single voxel within the visual cortex in a single subject during resting (darkness) and stimulated conditions. Changes in brain signal intensity occurring during cerebral transit of the high magnetic susceptibility $Gd(DTPA)^{2-}$ were converted to contrast agent concentration–time curves (*8, 13*). The area under the concentration-time curve, corrected for recirculation by gamma-variate fitting (*14*), is proportional to the local CBV (*15*). These calculations were performed on a voxel-by-voxel basis to generate images of relative CBV (*16*). The resulting resting and activated functional CBV images were subtracted to reveal areas involved in processing of the task.

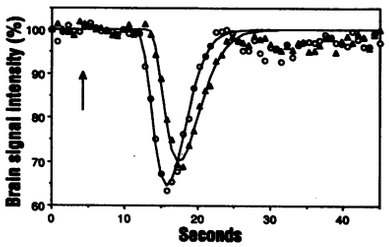

Fig. 2. Changes in NMR brain signal intensity during the first-pass transit of intravenously administered paramagnetic contrast agent (0.1 mmol/kg $Gd(DTPA)^{2-}$, at arrow). Sixty images were acquired in 45 seconds (▲, resting; ○, activated). Baseline normalized signal intensity changes from a single subject are shown for a single 3 by 3 by 10 mm voxel within the visual cortex during rest (darkness) and during 7.8-Hz photic stimulation. The activated state is characterized by a larger blood volume (area under curve).

Functional CBV and anatomic images from one subject are shown registered in Fig. 3. The CBV subtraction image (Fig. 3C) shows a marked area of increased blood volume in the primary visual cortex (V1). Moreover, demarcation of the activated region corresponds well to the anatomically determined gray-white borders. This result is in agreement with autoradiographic results in animals, which show sharp boundaries between functionally distinct regions (*2, 17*). During photic stimulation, each of our seven subjects showed a significant increase in regional blood volume occurring within the anatomically defined primary visual cortex (paired t test, $P < 0.001$), with an average increase (±SD) in CBV of 32 ± 10% (Table 1) (*18*). CBV subtraction images were used to estimate the extent of cortex activated by photic stimulation. Using a threshold 2 SDs above the mean of the subtraction images, we found the area of activated cortex to be 252 ± 87 mm^2 for the left hemisphere and 260 ± 175 mm^2 for the right (n = 7). The greatest CBV changes in all of our subjects were observed in the medial-posterior regions of the occipital lobes along the calcarine fissures. However, as has been reported by other groups, we also observed areas outside of area 17 that showed a >2 SD activation in several subjects. Some of these loci could be extrastriate visual areas. We did not include these regions in our calculations of V1 area, because their location was always outside the region of striate cortex (*5*).

A close association between activated cortical areas and the calcarine fissure was observed. However, anatomic images revealed a high degree of variability in location, orientation, and extent of the calcarine fissure. Functional CBV images reflect this anatomic variability as shown in Fig. 4, which displays center-of-mass coordinates and extents of the activated regions for each of our subjects in the common proportional coordinate system. Using the 3-D anatomic images, we directly measured the linear extent of the anteroposterior projection of the calcarine fissures: 36 ± 7 mm (left) and 33 ± 6 mm (right). Anteroposterior projection of the functional extents in Fig. 4 are not significantly different: 34 ± 9 mm (left) and 29 ± 14 mm (right). In addition to direct intrasubject correlation of active areas to their underlying anatomy, stereotactic results (Table 1 and Fig. 4) also demonstrate that NMR-determined regions of activity fall within PET-determined center-of-mass coordinates of the primary visual system (*5, 9*).

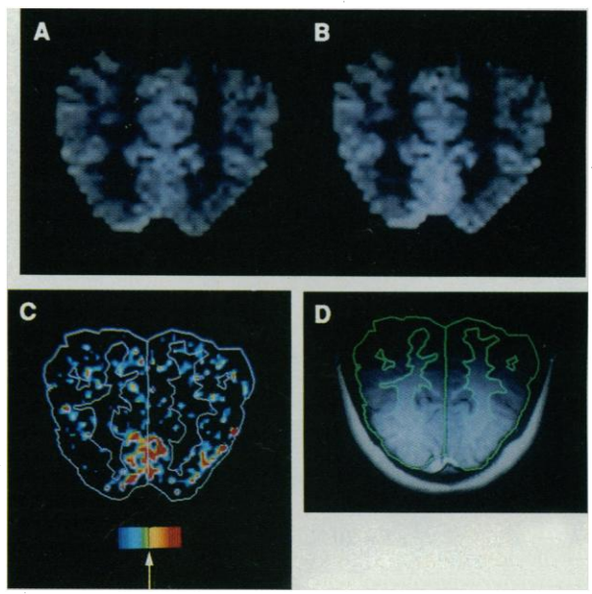

Fig. 3. Magnetic resonance CBV maps of the brain during darkness (**A**) and during 7.8-Hz photic stimulation (**B**). Image intensity is proportional to CBV. All images are aligned along the calcarine fissure (Fig. 1), with the occipital pole at the bottom. (**C**) Subtraction image of changes in CBV induced by photic stimulation (C = B − A). A linear color scale was used, with red equivalent to greatest activity. The arrow points to the +2 SD threshold. (**D**) An anatomic (T1-weighted) image was used to segment the gray and white matter (*20*). This outline was applied to the CBV subtraction image. A marked area (~600 mm^2) of increased blood volume (~24%) is localized in the anatomically defined primary visual cortex (C). We acquired these CBV images using a 3 by 3 by 10 mm voxel.

These experiments demonstrate the potential of magnetic resonance techniques for high-resolution mapping of brain areas involved in cognitive processing. Further improvements in both spatial resolution and sensitivity of the NMR method can be expected with the ongoing development of localized gradient coils and phased array receiver coils. The sensitivity of our NMR technique to changes in blood volume, as distinguished from changes in blood flow in previous radionuclide studies, offers the possibility of performing continuous serial imaging of cortical function with subsecond temporal resolution using intravascular contrast agents at equilibrium within the vascular space (*19*). The ability to acquire 2-D EPI images in times as short as 50 ms implies that one may be able to resolve changes within the hemodynamic response time of neural activation, ~100 ms (*3*). However, these studies depend on the availability of contrast agents for human use that exhibit a long intravascular half life. Magnetic resonance offers the combination of precise anatomical localization of function and complete 3-D imaging of the brain (*12*). The development of a standardized functional neuroanatomy will broaden our understanding of the unique structure-function relations involved in neural information processing.

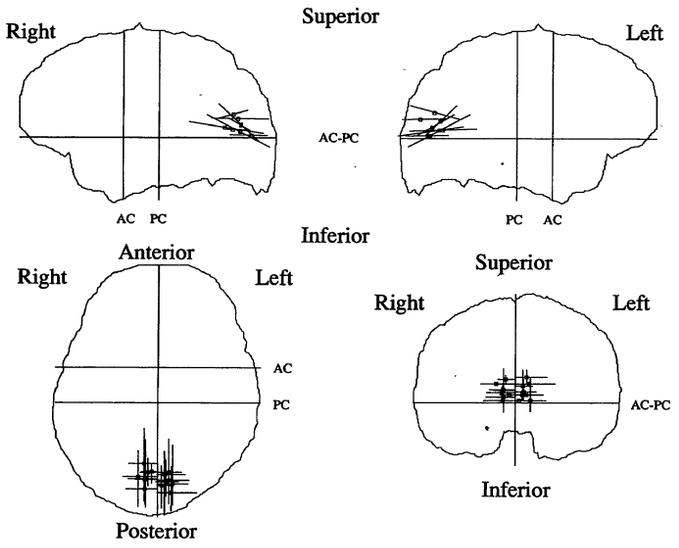

Fig. 4. Foci and extents of cortex showing increased blood volume during photic stimulation. Calculations were based on the regions defined by a threshold 2 SD above the mean of the subtraction images. Projection views of the center-of-mass and linear extent of activated cortex for each of our subjects are shown in standardized sagittal, axial, and coronal orientations. AC–PC distance equals 24.0 mm. Coordinates are listed in Table 1.

Table 1. Functional-anatomical location of primary visual cortex. We determined regions of interest (ROI), defining the areas of greatest change, from each subject's CBV subtraction image, using a threshold 2 SD above the mean. These ROI were used to determine the percent change and center-of-mass of activated cortex. Standardized proportional coordinates were determined relative to the AC-PC line (*11*). The point (0,0,0) is at the level of a line drawn between the anterior and posterior commissures (SI = 0), at the midline of the brain (RL = 0), and located anteroposteriorly halfway between the commissures (AP = 0). Regional CBV responses are expressed as percent change, after correction for global CBV variation (*5*). CBV percent change = [(CBV stimulated − CBV unstimulated)/(CBV unstimulated)] × 100.

Subject	CBV (% change)	Center of activation (mm)			
		Side	AP	SI	RL
1	40	L	−63	5	8
		R	−62	5	−4
2	24	L	−64	11	5
		R	−67	9	−8
3	21	L	−71	1	10
		R	−67	4	−8
4	21	L	−68	18	8
		R	−63	16	−6
5	48	L	−75	7	6
		R	−70	7	−12
6	39	L	−70	7	6
		R	−68	8	−8
7	30	L	−64	5	5
		R	−56	7	−9
Average ±SD	32 ± 10	L	−68 ± 5	8 ± 5	7 ± 2
		R	−65 ± 5	8 ± 4	−8 ± 2

REFERENCES AND NOTES

1. P. S. Churchland and T. J. Sejnowski, *Science* **242**, 741 (1988); S. M. Kosslyn, *ibid.* **240**, 1621 (1988); M. S. Gazzaniga, *ibid.* **245**, 947 (1989); M. I. Posner, S. E. Petersen, P. T. Fox, M. E. Raichle, *ibid.* **240**, 1627 (1988); N. C. Andreasen, *ibid.* **239**, 1381 (1988).
2. S. Zeki and S. Shipp, *Nature* **335**, 311 (1988).
3. C. A. Sandman, J. P. O'Halloran, R. Isenhart, *Science* **224**, 1355 (1984).
4. M. E. Phelps, D. E. Kuhl, J. C. Mazziotta, *ibid.* **211**, 1445 (1981); M. E. Raichle, in *Handbook of Physiology*, vol. 5 of *The Nervous System, Higher Functions of the Brain*, F. Plum, Ed. (American Physiological Society, Bethesda, MD, 1987), pp. 643–674; M. E. Phelps and J. C. Mazziotta, *Science* **228**, 799 (1985); S. E. Petersen, P. T. Fox, M. I. Posner, M. Mintun, M. E. Raichle, *Nature* **331**, 585 (1988).
5. P. T. Fox *et al.*, *Nature* **323**, 806 (1986); P. T. Fox, F. M. Miezin, J. M. Allman, D. C. Van Essen, M. E. Raichle, *J. Neurosci.* **7**, 913 (1987); P. T. Fox and M. E. Raichle, *J. Neurophysiol.* **51**, 1109 (1984); *Ann. Neurol.* **17**, 303 (1985).
6. M. A. Mintun, P. T. Fox, M. E. Raichle, *J. Cereb. Blood Flow Metab.* **9**, 96 (1989).
7. V. S. Caviness, P. A. Filipek, D. N. Kennedy, *Brain Dev.* **11**, 1 (1989); C. T. W. Moonen, P. C. M. van Zijl, J. A. Frank, D. Le Bihan, E. D. Becker, *Science* **250**, 53 (1990).
8. J. W. Belliveau, M. S. Cohen, R. M. Weisskoff, B. R. Buchbinder, B. R. Rosen, *J. Neuroimaging* **1**, 36 (1991); J. W. Belliveau *et al.*, *Magn. Reson. Med.* **14**, 538 (1990); B. R. Rosen, J. W. Belliveau, J. M. Vevea, T. J. Brady, *ibid.*, p. 249; B. R. Rosen, J. W. Belliveau, D. Chien, *Magn. Reson. Q.* **5**, 263 (1989).
9. C. J. Lueck *et al.*, *Nature* **340**, 386 (1989).
10. A. Villringer *et al.*, *Magn. Reson. Med.* **6**, 164 (1988).
11. J. Talairach *et al.*, *Atlas d'Anatomie Stereotaxique du Telencephale* (Masson, Paris, 1967); J. Talairach and P. Tournoux, *Co-Planar Stereotaxic Atlas of the Human Brain* (Thieme Medical Publishers, New York, 1988).
12. M. S. Cohen and R. M. Weisskoff, *Magn. Reson. Imaging* **9**, 1 (1991); R. R. Rzedzian and I. L. Pykett, *A.J.R.* **149**, 245 (1987); I. L. Pykett and R. R. Rzedzian, *Magn. Reson. Med.* **5**, 563 (1987); P. Mansfield, *J. Phys. C* **10**, L55 (1977).
13. C. R. Fisel *et al.*, *Magn. Reson. Med.* **17**, 336 (1991).
14. C. F. Starmer and D. O. Clark, *J. Appl. Physiol.* **28**, 219 (1970); H. K. Thompson, C. F. Starmer, R. E. Whalen, H. D. McIntosh, *Circ. Res.* **14**, 502 (1964).
15. L. Axel, *Radiology* **137**, 679 (1980); *Invest. Radiol.* **18**, 94 (1983); N. A. Lassen, O. Henriksen, P. Sejrsen, in *Handbook of Physiology*, vol. 3 of *The Cardiovascular System*, J. T. Shepherd and F. M. Abboud, Eds. (American Physiological Society, Bethesda, MD, 1983), pp. 21–63; N. A. Lassen, *J. Cereb. Blood Flow Metab.* **4**, 633 (1984).
16. We have used Monte Carlo simulations (R. M. Weisskoff, unpublished results) to estimate the accuracy in the CBV map on the basis of the signal-to-noise ratio (SNR) of the raw data. For our typical image SNR of 100:1 (3 by 3 by 10 mm voxel in V1) the CBV SNR would range from 30 to 40:1 depending on the patient. Therefore, we expect that our bolus method is sensitive to changes on the order of 3%. Measurement of absolute CBV, or blood flow, requires arterial input function sampling, which was not performed in these studies.
17. L. Sokoloff, Ed., *Brain Imaging and Brain Function* (Raven, New York, 1985).
18. The magnitude of these changes is larger than might be predicted from PET CBF studies and may be understood by noting that these previous studies likely underestimated the change in CBF due to the lower resolution of the PET images. The effect of partial volume averaging of the relatively thin enhancing and nonenhancing regions reduces the average change in CBF (*6*). The ability of NMR to acquire an oblique slice along the calcarine fissure further minimizes partial volume averaging effects. In addition, compared to PET CBV studies, ours is strictly a plasma volume measurement, as distin-

guished from a red blood cell (RBC) volume measurement. Plasma volume exhibits a greater change during physiologic stimulus than RBC volume does [F. Sakai *et al.*, *J. Cereb. Blood Flow Metab.* **5**, 207 (1985)].
19. M. E. Moseley *et al.*, in *Proceedings of the Society of Magnetic Resonance in Medicine Ninth Annual Meeting*, New York, 18 to 24 August 1990 (Society of Magnetic Resonance in Medicine, Berkeley, CA, 1990), p. 56; T. A. Kent *et al.*, *Am. J. Neuroradiol.* **10**, 335 (1989).
20. D. N. Kennedy, P. A. Filipek, V. S. Caviness, *IEEE Trans. Med. Imaging* **8**, 1 (1989).
21. Supported by National Public Health Service grants R01-HL39810, R01-CA40303, and P01-CA48729 and General Electric Corporation. J.W.B. thanks P. T. Fox for helpful discussions and the loan of the photic goggles.

28 March 1991; accepted 26 July 1991

Dynamic Organization of Developing Purkinje Cells Revealed by Transgene Expression

RICHARD J. SMEYNE, JOHN OBERDICK, KARL SCHILLING, ALBERT S. BERREBI, ENRICO MUGNAINI, JAMES I. MORGAN*

The cerebellum has many properties that make it a useful model for investigating neural development. Purkinje cells, the major output neurons of the cerebellar cortex, have drawn special attention because of the availability of biochemical markers and mutants that affect their development. The spatial expression of L7, a protein specific for Purkinje cells, and L7βGal, a gene expressed in transgenic mice that was constructed from the L7 promoter and the marker β-galactosidase, delineated bands of Purkinje cells that increased in number during early postnatal development. Expression of the transgene in adult *reeler* mutant mice, which show inverted cortical lamination, and in primary culture showed that the initial expression of L7 is intrinsic to Purkinje cells and does not depend on extracellular signals. This may reflect an underlying developmental map in cerebellum.

THE MURINE CEREBELLAR CORTEX has been widely used to investigate neural development because its structure is relatively simple and ordered, its developmental progression is well documented, and cell-specific markers and viable mutants that affect its maturation are available. In particular, considerable emphasis has been placed on determining the contributions of cell-intrinsic and -extrinsic mechanisms to the development of Purkinje cells, the major output neurons of the cerebellar cortex. Analysis of transplants (*1*) and chimeras (*2*) indicates that Purkinje cell development is largely autonomous of the environment. However, studies with biochemical markers have shown that Purkinje cell maturation is not synchronous (*3, 4*). This raises the questions of whether Purkinje cell development is ordered with respect to time and position and whether this process is cell-intrinsic. Using molecular markers for murine Purkinje cells, we have shown that these neurons follow a stereotypical developmental map that is largely dictated by cell-autonomous processes.

A strain of mice has been derived that carries a transgene (L7βGal) that directs expression of β-galactosidase almost exclusively to cerebellar Purkinje neurons (*5*). Therefore, we have used β-galactosidase activity to follow developmental events that occur in individual or entire populations of Purkinje cells. The developmental expression of the L7βGal transgene was determined in tissue sections and whole mounts of cerebella from normal and mutant mice heterozygous for L7βGal.

By embryonic day 14 (E14), the cerebellum already contains its complete complement of Purkinje cells (*6*). However, at E17, the earliest time at which the transgene product can be detected, only subpopulations of Purkinje cells express L7βGal in normal mouse cerebellum (Fig. 1A). Expression is localized to four parasagittal bands of Purkinje cells, two on each side of the midline. The most medial of these bands spans nearly the entire anterior-posterior extent of the cerebellum, whereas the lateral band is only present in the posterior area.

After E17, the number of Purkinje cells expressing the gene increased such that all cells were L7βGal-positive by postnatal day 9 (P9) (Fig. 1, D and F). The induction of L7βGal after E17 occurred in a stereotyped topographical and temporal manner (Fig. 1). At P0 (day of birth), three bilateral bands (two medial and one lateral) were evident (Fig. 1, B and E). The medial bands were thicker in the posterior cerebellum, and the most lateral band was discontinuous (Fig. 1E). From P0 to P3, the pattern of gene expression did not change. At P4, the number of major bilateral parasagittal bands in the transgenic cerebellum had increased from three to five (two medial and three lateral) (Fig. 1C).

At all developmental stages, L7βGal and L7 were expressed in the same population of cells (Fig. 2, C and D). From P4 to P7, all Purkinje cells in the vermis became L7βGal- and L7-positive, whereas most of those in the lateral parts of the hemisphere were still negative. By P9, all Purkinje cells expressed the L7 gene and the L7βGal transgene (Fig. 1, D and F) (*4*). This inductive pattern of L7βGal was stereotyped: the initial expression was posteromedial, and expression progressed anteriorly and then laterally. Two other Purkinje cell markers, PEP-19 and calbindin 28kD (*7*), did not show the same banding pattern as that revealed by L7 in normal cerebellum (Fig. 3, A to C). Nevertheless, antibodies to calbindin 28kD and PEP-19 stain clusters of Purkinje cells early in development (*3, 4*).

In the central nervous system of the homozygous *reeler* mouse, there is an inversion of lamination, most likely a consequence of an abnormality in neuronal migration (*8*). In the cerebellum this results in Purkinje cells that are incorrectly positioned and largely organized into clusters (*9*). Therefore, we could test the effect of cell position on L7 expression by examining L7βGal expression in *reeler* mice. In adult *reeler* mice, all Purkinje cells expressed L7βGal (Fig. 2B). However, two bilateral bands of Purkinje cells expressed large amounts of the transgene, whereas Purkinje cells located medial and lateral to these bands expressed smaller amounts of the transgene (Fig. 2B). This is in contrast to expression in wild-type adult cerebellum, which was uniform throughout (Fig. 2A).

Although it is difficult to make direct comparisons between *reeler* and wild-type cerebella because of the lack of foliation in *reeler*, several features of transgene expression are apparent. (i) The initial induction of L7βGal expression in Purkinje cells is the same in *reeler* and wild-type cerebellum (Fig. 2E). (ii) As in wild-type cerebellum, the expression of L7βGal is concentrated in medial Purkinje cells during early postnatal development (compare Fig. 1, A through C, to Fig. 2, E through H). (iii) In contrast to the situation in wild-type mice, in *reeler* mice the amount of L7βGal decreases with age in

R. J. Smeyne, Department of Neurosciences, Roche Institute of Molecular Biology, Roche Research Center, Nutley, NJ 07110, and Department of Neuroscience, University of Medicine and Dentistry of New Jersey, Newark, NJ 07103.
J. Oberdick, K. Schilling, J. I. Morgan, Department of Neurosciences, Roche Institute of Molecular Biology, Roche Research Center, Nutley, NJ 07110.
A. S. Berrebi and E. Mugnaini, Graduate Degree Program in Biobehavioral Sciences, Laboratory of Neuromorphology, University of Connecticut, Storrs, CT 06269.

*To whom correspondence should be addressed.